J Nanopart Res (2017) 19: 377
https://doi.org/10.1007/s11051-017-4070-9

RESEARCH PAPER

Thermosensitive polymer stabilized core-shell AuNR@Ag nanostructures as "smart" recyclable catalyst

Dongxiang Li · Na Liu · Yuanyuan Gao · Weihong Lin · Chunfang Li

Received: 29 August 2017 / Accepted: 30 October 2017 / Published online: 15 November 2017

Abstract Core-shell AuNR@Ag nanostructures were synthesized and surface-grafted with thermosensitive poly(*N*-isopropylacrylamide) to enhance stability and endow stimuli-responsive property. The AuNR cores showed average dimensions of 8-nm diameter and 33-nm length, while the anisotropic silver shells displayed 1–2 nm thin side and maximal 8 nm fat side. The obtained polymer-stabilized AuNR@Ag nanostructures as catalysts showed normal Arrhenius change of apparent rate constant, k_{app}, in catalyzed reaction between 20 and 30 °C, but displayed a decrease of k_{app} with respect to the temperature increasing between 32.5–40 °C, showing self-inhibition of the observed catalytic activity. Such "smart" self-inhibition of catalytic activity at enhanced temperature can be attributed to the thermosensitive response of the grafted polymer molecules and should be significant to control the reaction rate and avoid superheat for exothermic reactions. Such polymer-stabilized nanocatalyst also could be recovered and reused in the catalytic system.

D. Li (✉)
State Key Laboratory Base of Eco-chemical Engineering, Lab of Colloids and Functional Nanostructures, Qingdao University of Science and Technology, Qingdao 266042, China
e-mail: lidx@iccas.ac.cn

N. Liu · Y. Gao · W. Lin · C. Li (✉)
College of Chemistry and Molecular Engineering, Qingdao University of Science and Technology, Qingdao 266042, China
e-mail: lichunfang@qust.edu.cn

Keywords Nanostructures · Gold · Silver · Thermosensitive polymer · Catalyst

Introduction

Gold nanorods (AuNRs) have been widely employed as special nanosupport to fabricate excellent core-shell bimetallic nanostructures with platinum (Feng et al. 2008; Grzelczak et al. 2006; He et al. 2011; Lu et al. 2010b), silver (Cho et al. 2010; Ma et al. 2014; Xiang et al. 2008), and palladium in catalyst applications (Bi et al. 2015; Lu et al. 2017; Ortiz et al. 2017; Zhang et al. 2009). The coexistence of two metals in these bimetallic nanostructures alters their electronic energy band and surface distribution by the intermetallic electron transfer, so they display superior catalytic activity as catalysts due to the synergistic effect (Guo et al. 2012; Jiang and Xu 2011; Lu et al. 2010a; Wang and Li 2011). Generally, these bimetallic nanostructures are synthesized by surfactant-assisted seed growth method and the obtained nanostructures are originally stabilized by surfactant molecules (Feng et al. 2008; Xiang et al. 2008). However, the surfactant stabilizer will be removed in the catalysis process when the metal nanostructures are used as catalysts, which will usually make the nanocatalysts aggregate into precipitates after reaction due to the large surface energy of metal nanoparticles.

To our knowledge, grafting polymers on the metal nanoparticles can decrease the nanoparticle surface energy

and provide steric stabilization to avoid the nanoparticle aggregation (Chen and Klok 2013; Li et al. 2009). Remarkably, stimuli-responsive polymers can endow fascinating "smart" properties to the grafted nanoparticles (Li et al. 2007; Lu et al. 2006; Wang et al. 2016; Zhang et al. 2014). Therefore, in this work, a temperature-responsive polymer, poly(*N*-isopropylacrylamide) (PNIPAM), was selected to graft the nanostructures of AuNR core and Ag shell (AuNR@Ag) to provide stabilization and thermal sensitivity. It was found that the fabricated PNIPAM-stabilized AuNR@Ag nanostructures showed "smart" self-inhibition catalytic activity at enhanced temperature, and they were also found to be recyclable catalysts.

Methodology and experimental

AuNR@Ag nanostructures

The core-shell AuNR@Ag nanostructures were synthesized from AuNRs by a surfactant-assisted seed-growth approach (Becker et al. 2008; Xiang et al. 2008). The AuNRs were aforehand prepared according to the previous works (Bai et al. 2009; Li et al. 2011; Nikoobakht and El-Sayed 2003), which were purified by centrifugation and redispersed in 1 mM hexadecyltrimethylammonium bromide (CTAB). Then, 20 mL above suspension of AuNRs (containing approx. 150 μmol Au atoms) was mixed with 150 mL CTAB solution (0.1 M), 15 mL ascorbic acid (50 mM), and a proper volume of NaOH solution (0.1 M) to adjust pH to about 9. Finally, 15 mL $AgNO_3$ (5 mM, 75 μmol Ag atoms) was added into the mixture and thereafter a continuous growth of Ag shell on the surface of AuNRs was performed for about 30 min until the system color changed into dark cyan.

Polymer-stabilized AuNR@Ag

The above AuNR@Ag nanostructures were purified by centrifugation twice and subsequently incubated with 275 mL solution of sulfur-terminated PNIPAM (0.2 mg/mL, Mw ~ 25,000) overnight at 30 °C to perform PNIPAM grafting via the formation of Au–S bonds. The PNIPAM-stabilized AuNR@Ag nanostructures were then separated from the mixture and further purified twice by centrifugation with 14,000 rpm at 25 °C to discard the ungrafted polymer in the mixture.

Catalytic activity

The catalytic activity of silver shell of the AuNR@Ag samples was checked in the reduction of 4-nitrophenol to aminophenol by sodium borohydride (Li et al. 2007; Zhang et al. 2014). Detaily, 2.3 mL aqueous solution of 0.15 mM 4-nitrophenol was mixed with 50 μL suspension of the naked AuNR@Ag or PNIPAM-stabilized AuNR@Ag sample (containing 0.045 μmol Ag atoms), then 250 μL ice-cold $NaBH_4$ solution (100 mM) was added into the system which was immediately monitored by a characteristic absorbance of the reactant at 400 nm. The catalytic reaction was performed at different temperature from 20 to 40 °C with an interval of 2.5 °C.

Characterization and instrumentation

UV-vis spectra of AuNR@Ag samples and real-time absorbance of 4-nitrophenol at 400 nm in the catalytic reaction were recorded on a PERSEE TU1901 spectrometer (Beijing Purkinje General, China) which was equipped with a circulating water bath (Bluepard MP-13H, Shanghai Yiheng Technical Co., Ltd) to control the system temperature (errors ± 0.1 °C). X-ray photoelectron spectroscopy (XPS) was measured on a ESCALab220i-XL instrument (VG Scientific). Transition electronic microscopic (TEM) images were obtained on a JEM-2100 microscope (JEOL, Japan). The centrifugation was performed on a Sigma 3K15 centrifuge (Germany), and the used PNIPAM-stabilized AuNR@Ag catalyst was recovered by centrifugation with 14,000 rpm at 35 °C for more than 4 h totally.

Results and discussion

Characterization of PNIPAM-stabilized AuNR@Ag nanostructures

Optical photo and UV-vis spectra of the obtained AuNRs, AuNR@Ag nanostructures, and PNIPAM-stabilized AuNR@Ag nanostructures are shown in Fig. 1a, b. It is found that the initial AuNRs is reddish brown (Fig. 1a) and changes into dark cyan after the growth of silver shells. The color of the PNIPAM-stabilized AuNR@Ag nanostructures is very similar to

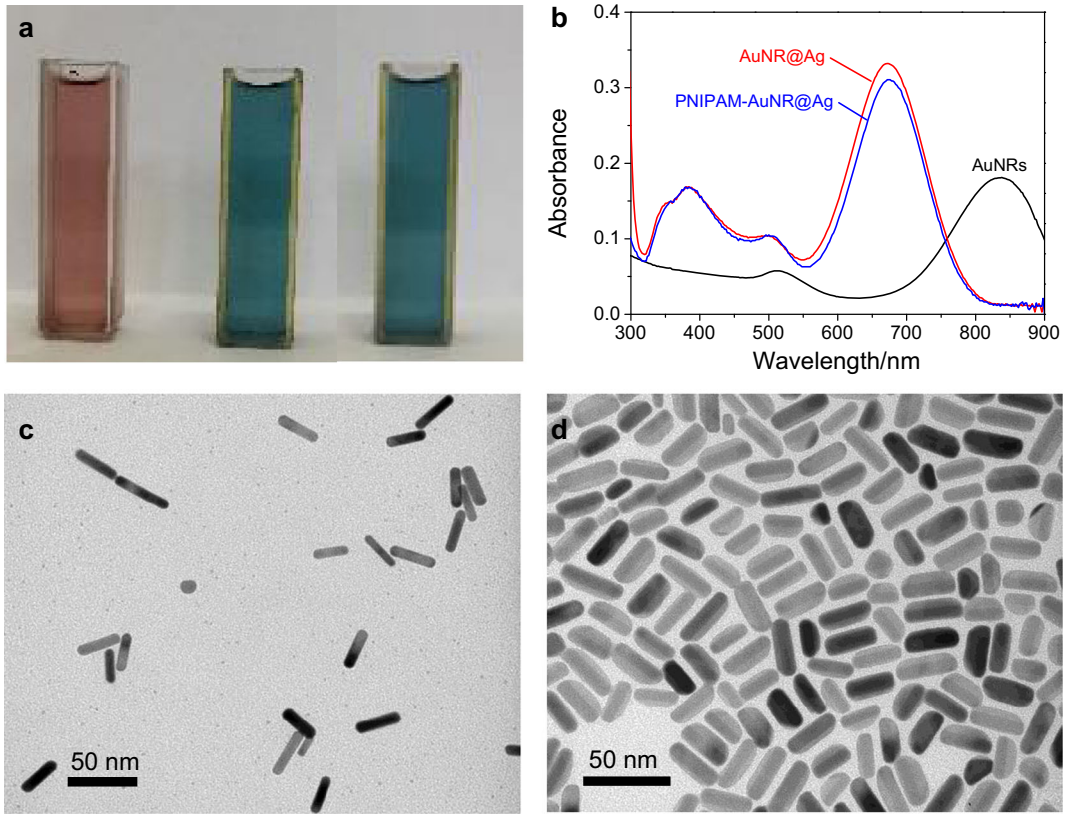

Fig. 1 **a**–**b** Optical photo (**a**) and UV-vis spectra (**b**) of AuNRs (left in **a**), AuNR@Ag (middle in **a**), and PNIPAM-stabilized AuNR@Ag nanostructures (right in **a**); **c**–**d** TEM images of AuNRs (**c**) and AuNR@Ag nanostructures (**d**)

the naked AuNR@Ag samples. Correspondingly, the characteristic longitude and transverse surface plasmon resonance (SPR) peaks of AuNRs in the UV-vis spectrum (Fig. 1b) focus around 835 and 510 nm, respectively. However, the AuNR@Ag nanostructures show more complex extinction spectrum (Dai et al. 2017; Li et al. 2008). The sharp absorbance at 672 nm corresponds the longitude SPR band of AuNRs with the combination of silver coating. The broad peak between 320 and 450 nm (focusing 385 nm) is ascribed to the SPR of silver shell. The modification by sulfur-terminated PNIPAM only brings 2 nm redshift of longitude SPR absorbance to 674 nm, this should be ascribed to the formation of Au–S bonds. Figure 1c, d shows TEM images of the as-prepared AuNRs and the AuNR@Ag nanostructures. The initial AuNRs in Fig. 1c shows well-dispersed state with average dimensions of 8-nm diameter and 33-nm length (i.e., an aspect ratio of 4.1), which is in accordance with the wavelength of longitude SPR band. For AuNR@Ag nanostructures in Fig. 1d, an anisotropic coating on the surface of the AuNRs is apparent because the thickness of Ag shell at the two sides of gold nanorod is obviously different. The thin side of silver shell is only 1–2 nm and the fatter side is maximally 8 nm. Such an anisotropic Ag shell can be ascribed to the dominant side of 110 facet for silver growth (Xiang et al. 2008).

Noticeably, X-ray photoelectron spectroscopy (XPS) survey scan of the PNIPAM-stabilized AuNR@Ag nanostructures in Fig. 2a reveals the presence of Au (2.3% by atom), Ag (7.4%), C (47.5%), N (24%), O (17%), Br (1.3%), and trace sulfur. The detectable content of silver is higher than gold; this should be due to the coverage/encapsulation of silver to gold core. The observed binding energies at 83.9 and 87.6 eV in the enlarged XPS spectra (Fig. 2b) correspond to metallic Au $4f_{7/2}$ and $Au4f_{5/2}$ spin-orbit split states; whereas, those at 367.9 and 373.9 eV correspond to metallic Ag $3d_{5/2}$ and Ag $3d_{3/2}$ states, respectively. The

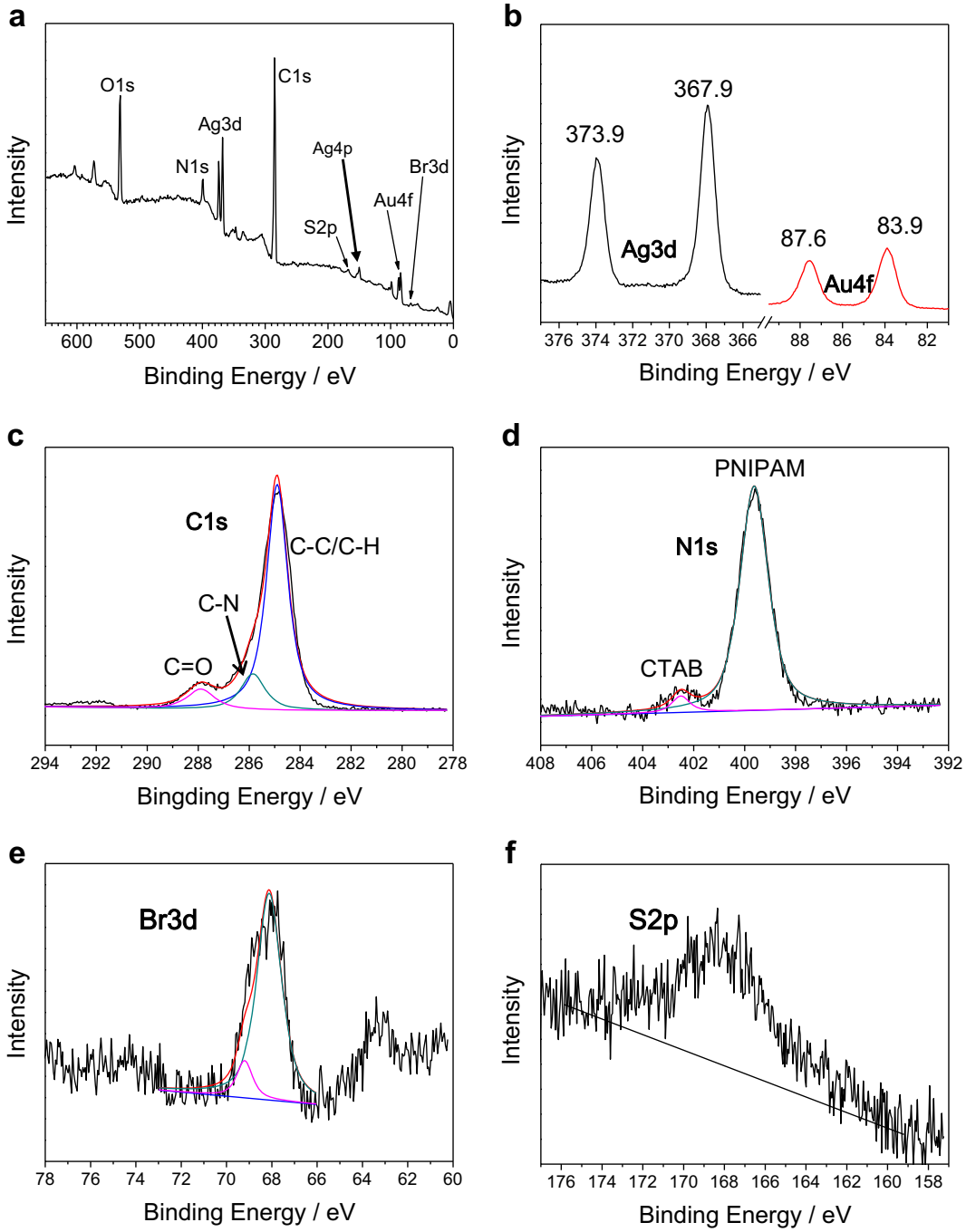

Fig. 2 XPS survey scan (**a**), Au 4f and Ag 3d (**b**), C 1s (**c**), N 1s (**d**), and Br 3d (**e**) deconvolution analysis, and S2p (**f**) spectrum of the PNIPAM-stabilized AuNR@Ag nanostructures

deconvolution of C1s spectrum in Fig. 2c shows three discernible peaks with binding energies of 284.9, 286.1, and 287.9 eV. If these three peaks are mainly attributed to carbon atoms in C–H/C–C, C–N, and amide bonds in PNIPAM, their integral ratio from the deconvolution (approximately 8.5:1.6:1) differs from the theoretical value of 4:1:1. This implies the presence of other component which should be residual CTAB in suspension and adsorbed CTAB on nanostructure surface. Moreover, the deconvolution of N 1s (Fig. 2d) shows major

acrylamide bond (399.6 eV) in PNIPAM and minor quaternary ammonium ions (402.5 eV) in CTAB; the deconvolution of Br3d spectrum (Fig. 2e) also shows main existence of covalent Br in PNIPAM (68.1 eV) and minor ionic Br in CATB (69.2 eV). In addition, an observable signal from sulfur at 162.2 eV (Fig. 2f) further verifies successful grafting of PNIPAM to AuNR@Ag surface.

Thermosensitive catalytic activity

The catalytic activity of silver nanoparticles were typically detected via a catalytic reduction of 4-nitrophenol by $NaBH_4$ (Li et al. 2007; Zhang et al. 2014). In this work, the catalytic activity of the naked AuNR@Ag and the PNIPAM-stabilized AuNR@Ag samples was checked similarly. The used molar ratio of $NaBH_4$ to 4-nitrophenol was about 73; thus, the concentration of $NaBH_4$ could be taken as a constant throughout the reaction and first-order rate kinetics could be assumed with respect to the concentration, c, of 4-nitrophenol. The catalytic kinetic curves of 4-nitrophenol reduction catalyzed by the naked AuNR@Ag and the PNIPAM-stabilized AuNR@Ag nanostructures at different temperature were shown in Fig. 3a, b, respectively. Obviously, there is a linear relationship between $\ln[c/c_0]$ and reaction time, t, from 20 to 40 °C, where c_0 is the original concentration of 4-nitrophenol initially. It has been shown that the activation/introduction period of this catalytic reaction strongly depends on the reaction temperature, which is in accordance with the previous work (Li et al. 2007). The activation/introduction period is shorter for the naked AuNR@Ag (Fig. 3a) than the PNIPAM-stabilized AuNR@Ag (Fig. 3b); this can be ascribed to the partial coverage of silver surface by PNIPAM in the latter case. The apparent rate constant, k_{app}, can be calculated by linearly fitting $\ln[c/c_0]$ to t based on the first-order reaction as listed in Table 1. Obviously, k_{app} for the PNIPAM-stabilized AuNR@Ag catalyst is lower than that of

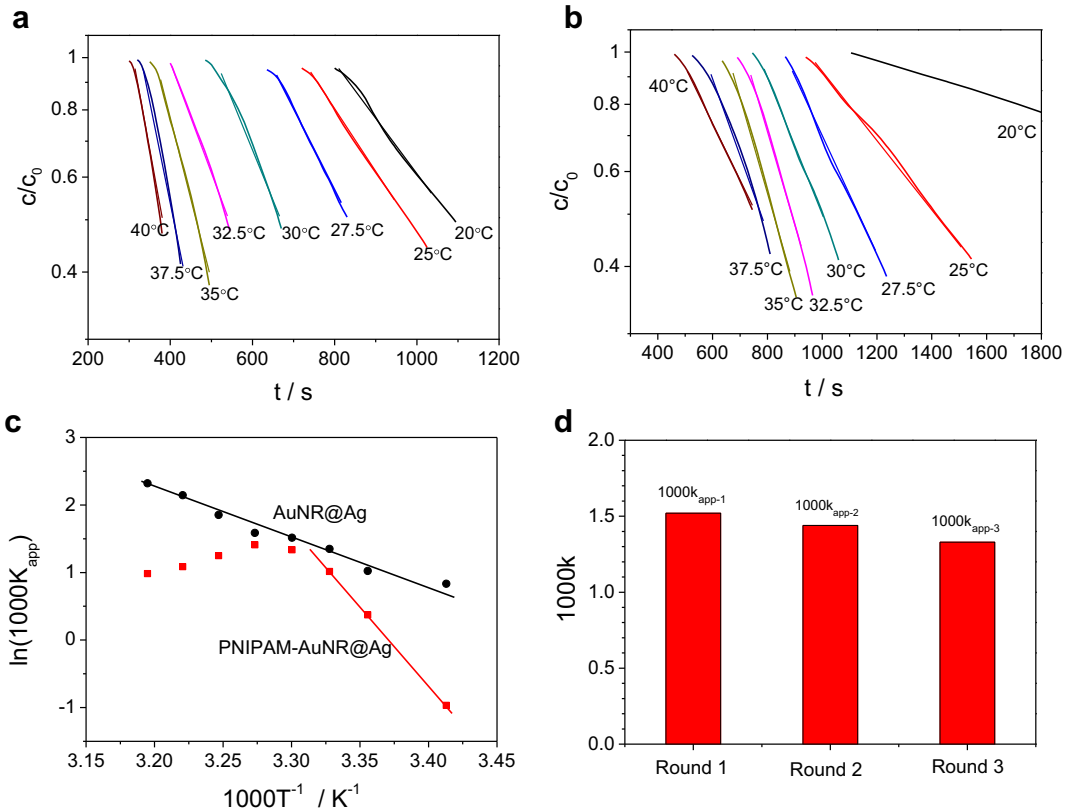

Fig. 3 **a**–**b** Kinetics of 4-nitrophenol reduction catalyzed by AuNR@Ag (**a**), PNIPAM-stabilized AuNR@Ag nanostructures (**b**) at different temperature with fitted lines; **c** Arrhenius plots of the apparent rate constant, k_{app}, in **a** and **b**; **d** k_{app} values in the first use and twice recycle uses of PNIPAM-stabilized AuNR@Ag catalyst

Table 1 The calculated apparent rate constant, k_{app}, at different temperature

Temperature/°C	$k_{app,\ naked\ AuNR@Ag}/10^{-3}\ s^{-1}$	$k_{app,\ PNIPAM\text{-}stabilized\ AuNR@Ag}/10^{-3}\ s^{-1}$
20.0	2.30	0.38
25.0	2.78	1.52
27.5	3.85	2.76
30.0	4.55	3.8
32.5	4.88	4.09
35.0	6.38	3.49
37.5	8.53	2.96
40.0	10.2	2.67

the naked AuNR@Ag sample; this can be also ascribed to the partial coverage of silver surface by polymer. For the naked AuNR@Ag catalyst, k_{app} gradually increases from 0.0023 to 0.0102 s^{-1} from 20 to 40 °C, while for the PNIPAM-stabilized AuNR@Ag catalyst, it first increases from 0.00038 to 0.00409 s^{-1} from 20 to 32.5 °C. Then, it is interesting that k_{app} value decreases slowly to 0.00267 s^{-1} from 32.5 to 40 °C.

Figure 3c gives the Arrhenius plot of k_{app} at different temperatures, T. For the naked AuNR@Ag catalyst, it shows that a change of k_{app} value obviously obeys the Arrhenius linear relationship between $\ln k_{app}$ and T^{-1}. However, for the PNIPAM-stabilized AuNR@Ag catalyst, k_{app} value quite differs from the linear Arrhenius relationship between $\ln k_{app}$ and T^{-1}. First, at low temperature between 20 and 27.5 °C, k_{app} value perfectly obeys Arrhenius linear relationship. Then, a tiny negative deviation occurs at 30 °C, because the grafted PNIPAM begins to thermosensitive shrink via the conformational change of polymer chains. Thereafter, k_{app} value reaches to a maximum value at 32.5 °C, which corresponds the lower critical solution temperature (LCST) of PNIPAM (Li et al. 2007; Zhang et al. 2014). Finally, from 32.5 to 40 °C, k_{app} value decreases slowly with respect to temperature increasing, this should be ascribed to the coverage of shrunk polymer chains on silver surface. The polymer shrinkage on silver shell covers a part of silver surface and also prevent diffusion of reactant substance, so that "apparent" self-inhibition of catalytic activity occurs at above 32.5 °C. Such "smart" self-inhibition of catalytic activity at enhanced temperature is particularly significant for an exothermic reaction to control the reaction rate and avoid the reaction superheat.

Catalyst recovery and recycle use

On the other hand, the polymer grafting on the AuNR@Ag nanostructures was designed to endow steric stabilization and possibly brought recyclable nanocatalysts. Factually, the PNIPAM-stabilized AuNR@Ag could be recovered by centrifugation, redispersed and reused in the catalytic reaction, but the naked AuNR@Ag was indeed found to aggregate into black precipitates in centrifugation and could not be redispersed well even by ulstrasonication. Figure 3d shows k_{app} value of the PNIPAM-stabilized AuNR@Ag catalyst in the first use and twice recycle uses at 25 °C. The k_{app} value in the first use is 0.00152 s^{-1}, that in the second use and third use are respectively 0.00144 and 0.00133 s^{-1}, remaining 95 and 88% of the catalytic activity. The decrease of catalytic activity can be attributed to the loss of nanoparticles in the recovery by centrifugation. Therefore, the polymer stabilization make the metal nanocatalyst be recyclable.

Conclusions

In summary, core-shell AuNR@Ag nanostructures were stabilized by thermosensitive PNIPAM. The obtained polymer-stabilized nanostructures as catalysts showed normal Arrhenius change of apparent rate constant, k_{app}, of catalyzed reaction between 20 and 30 °C, but displayed a decrease of k_{app} with respect to the temperature increasing between 32.5 and 40 °C. Such "smart" self-inhibition of catalytic activity at enhanced temperature can be attributed to the thermal-responsive shrink of the grafted polymer chains, and it should be significant to control the reaction rate and avoid superheat of exothermic reactions. The polymer-stabilized nanocatalyst can be considered as a recyclable catalyst, and the polymer stabilization strategy can be generalized to many other metal nanocatalysts.

Funding information This work was financially supported by the National Natural Science Foundation of China (NNSFC 21273123) and the Key Research and Development Projects (2016GGX102027) of Shandong Province, China.

Compliance with ethical standards

Conflict of interest The authors declare that they have no conflicts of interest.

References

Bai XT, Gao YA, Liu HG, Zheng LQ (2009) Synthesis of amphiphilic ionic liquids terminated gold nanorods and their superior catalytic activity for the reduction of nitro compounds. J Phys Chem C 113:17730–17736. https://doi.org/10.1021/jp906378d

Becker J, Zins I, Jakab A, Khalavka Y, Schubert O, Sönnichsen C (2008) Plasmonic focusing reduces ensemble linewidth of silver-coated gold nanorods. Nano Lett 8:1719–1723. https://doi.org/10.1021/nl080720k

Bi CX, Feng C, Miao TT, Song YH, Wang DY, Xia HB (2015) Understanding the effect of ultrathin AuPd alloy shells of irregularly shaped Au@AuPd nanoparticles with high-index facets on enhanced performance of ethanol oxidation. Nanoscale 7:20105–20116. https://doi.org/10.1039/C5NR06035D

Chen L, Klok HA (2013) "Multifaceted" polymer coated, gold nanoparticles. Soft Matter 9:10678–10688. https://doi.org/10.1039/c3sm51789f

Cho EC, Camargo PHC, Xia Y (2010) Synthesis and characterization of noble-metal nanostructures containing gold nanorods in the center. Adv Mater 22:744–748. https://doi.org/10.1002/adma.200903097

Dai H, Zhang L, Wang Z, Wang X, Zhang J, Gong H, Han J-B, Han Y (2017) Linear and nonlinear optical properties of silver-coated gold nanorods. J Phys Chem C 121:12358–12364. https://doi.org/10.1021/acs.jpcc.7b00295

Feng L, Wu X, Ren L, Xiang Y, He W, Zhang K, Zhou W, Xie S (2008) Well-controlled synthesis of Au@Pt nanostructures by gold-nanorod-seeded growth. Chem Eur J 14:9764–9771. https://doi.org/10.1002/chem.200800544

Grzelczak M, Perez-Juste J, Rodriguez-Gonzalez B, Liz-Marzan LM (2006) Influence of silver ions on the growth mode of platinum on gold nanorods. J Mater Chem 16:3946–3951. https://doi.org/10.1039/b606887a

Guo X, Zhang Q, Sun Y, Zhao Q, Yang J (2012) Lateral etching of core–shell Au@metal nanorods to metal-tipped Au nanorods with improved catalytic activity. ACS Nano 6:1165–1175. https://doi.org/10.1021/nn203793k

He W, Liu Y, Yuan J, Yin J-J, Wu X, Hu X, Zhang K, Liu J, Chen C, Ji Y, Guo Y (2011) Au@Pt nanostructures as oxidase and peroxidase mimetics for use in immunoassays. Biomaterials 32:1139–1147. https://doi.org/10.1016/j.biomaterials.2010.09.040

Jiang H-L, Xu Q (2011) Recent progress in synergistic catalysis over heterometallic nanoparticles. J Mater Chem 21:13705–13725. https://doi.org/10.1039/C1JM12020D

Li DX, Cui Y, Wang KW, He Q, Yan XH, Li JB (2007) Thermosensitive nanostructures comprising gold nanoparticles grafted with block copolymers. Adv Funct Mater 17:3134–3140. https://doi.org/10.1002/adfm.200700427

Li DX, He Q, Li JB (2009) Smart core/shell nanocomposites: intelligent polymers modified gold nanoparticles. Adv Colloid Interf Sci 149:28–38. https://doi.org/10.1016/j.cis.2008.12.007

Li DX, Jang YJ, Lee J, Lee JE, Kochuveedu ST, Kim DH (2011) Grafting poly(4-vinylpyridine) onto gold nanorods toward functional plasmonic core-shell nanostructures. J Mater Chem 21:16453–16460. https://doi.org/10.1039/c1jm13302k

Li M, Zhang ZS, Zhang X, Li KY, Yu XF (2008) Optical properties of Au/Ag core/shell nanoshuttles. Opt Express 16:14288–14293. https://doi.org/10.1364/OE.16.014288

Lu BB, Kan CX, Ke SL, Xu HY, Ni Y, Wang CS, Shi DN (2017) Geometry-dependent surface plasmonic properties and dielectric sensitivity of bimetallic Au@Pd nanorods. Plasmonics 12:1183–1191. https://doi.org/10.1007/s11468-016-0374-3

Lu C-L, Prasad KS, Wu H-L, Ho J-aA, Huang MH (2010a) Au nanocube-directed fabrication of Au−Pd core−shell nanocrystals with tetrahexahedral, concave octahedral, and octahedral structures and their electrocatalytic activity. J Am Chem Soc 132:14546–14553. https://doi.org/10.1021/ja105401p

Lu Y, Mei Y, Drechsler M, Ballauff M (2006) Thermosensitive core-shell particles as carriers for Ag nanoparticles: modulating the catalytic activity by a phase transition in networks. Angew Chem Int Ed 45:813–816. https://doi.org/10.1002/anie.200502731

Lu Y, Yuan J, Polzer F, Drechsler M, Preussner J (2010b) In situ growth of catalytic active Au−Pt bimetallic nanorods in thermoresponsive core−shell microgels. ACS Nano 4:7078–7086. https://doi.org/10.1021/nn102622d

Ma Y, Zhou J, Shu L, Li T, Petti L, Mormile P (2014) Optimizing Au/Ag core–shell nanorods: purification, stability, and surface modification. J Nanopart Res 16:2439. https://doi.org/10.1007/s11051-014-2439-6

Nikoobakht B, El-Sayed MA (2003) Preparation and growth mechanism of gold nanorods (NRs) using seed-mediated growth method. Chem Mat 15:1957–1962. https://doi.org/10.1021/cm0207321

Ortiz N, Hong SJ, Fonseca F, Liu Y, Wang GF (2017) Anisotropic overgrowth of palladium on gold nanorods in the presence of salicylic acid family additives. J Phys Chem C 121:1876–1883. https://doi.org/10.1021/acs.jpcc.6b12024

Wang D, Li Y (2011) Bimetallic nanocrystals: liquid-phase synthesis and catalytic applications. Adv Mater 23:1044–1060. https://doi.org/10.1002/adma.201003695

Wang Y, Feng AC, Yuan JY (2016) Application of stimuli-responsive polymer in catalyst systems of gold nanoparticles. Prog Chem 28:1054–1061. https://doi.org/10.7536/pc160217

Xiang YJ, Wu XC, Liu DF, Li ZY, Chu WG, Feng LL, Zhang K, Zhou WY, Xie SS (2008) Gold nanorod-seeded growth of silver nanostructures: from homogeneous coating to anisotropic coating. Langmuir 24:3465–3470. https://doi.org/10.1021/la702999c

Zhang C, Li C, Chen Y, Zhang Y (2014) Synthesis and catalysis of Ag nanoparticles trapped into temperature-sensitive and conductive polymers. J Mater Sci 49:6872–6882. https://doi.org/10.1007/s10853-014-8389-7

Zhang K, Xiang YJ, Wu XC, Feng LL, He WW, Liu JB, Zhou WY, Xie SS (2009) Enhanced optical responses of Au@Pd core/shell nanobars. Langmuir 25:1162–1168. https://doi.org/10.1021/la803060p